PRIMARY RESEARCH PAPER

Estimating specific inherent optical properties of tropical coastal waters using bio-optical model inversion and in situ measurements: case of the Berau estuary, East Kalimantan, Indonesia

**W. Ambarwulan · M. S. Salama ·
C. M. Mannaerts · W. Verhoef**

Abstract Specific inherent optical properties (SIOP) of the Berau coastal waters were derived from in situ measurements and inversion of an ocean color model. Field measurements of water-leaving reflectance, total suspended matter (TSM), and chlorophyll a (Chl a) concentrations were carried out during the 2007 dry season. The highest values for SIOP were found in the turbid waters, decreasing in value when moving toward offshore waters. The specific backscattering coefficient of TSM varied by an order of magnitude and ranged from $0.003 \ \mathrm{m^2 \ g^{-1}}$, for clear open ocean waters, to $0.020 \ \mathrm{m^2 \ g^{-1}}$, for turbid waters. On the other hand, the specific absorption coefficient of Chl a was relatively constant over the whole study area and ranged from $0.022 \ \mathrm{m^2 \ mg^{-1}}$, for the turbid shallow estuary waters, to $0.027 \ \mathrm{m^2 \ mg^{-1}}$, for deeper shelf edge ocean waters. The spectral slope of colored dissolved organic matter light absorption was also derived with values ranging from 0.015 to $0.011 \ \mathrm{nm^{-1}}$. These original derived values of SIOP in the Berau estuary form a corner stone for future estimation of TSM and Chl a concentration from remote sensing data in tropical equatorial waters.

Keywords Subsurface irradiance reflectance · Total suspended matter · Chlorophyll a · Ocean optics · Bio-optical model · Tropical waters

W. Ambarwulan · M. S. Salama ·
C. M. Mannaerts (✉) · W. Verhoef
Faculty of Geo-Information Science and Earth
Observation (ITC), University of Twente, Enschede,
The Netherlands
e-mail: mannaerts@itc.nl

W. Ambarwulan
National Coordinating Agency for Surveys and Mapping,
Cibinong, Indonesia

Introduction

The Berau estuary is a complex inlet lying off the Makassar Strait which consists of river deltas in the west and a barrier reef in the east. The area is a region of freshwater influence where the outflows of the Berau river and a number of smaller rivers (i.e., Sesayap and Lungsurannaga) mix with waters originating from the Pacific ocean through the Makassar strait. The dynamics of river discharges to the Berau estuary affect the spatial and temporal dynamics of water constituents causing small-scale patchiness in addition to the dynamic variability of the tidal currents. Berau estuary is located in the Indonesian Through Flow (ITF) and ENSO regions, which affect this tropical area with centers of action at around Indonesia - North Australia and the southern Pacific (Glantz et al., 1991). The positions of these large weather systems also affect cloud coverage. Diurnal clouds that develop in the tropical area significantly influence the energy and radiation budget through diffusion and absorption in the solar spectrum (Sharkov, 1998).

Over the year, the Makassar Strait has been extensively surveyed, and detailed descriptions have been published especially related to the ITF, a deep ocean current also important in regional and global climate studies (Hautala et al., 2001; Gordon et al., 1999; Susanto et al., 2006). However, only limited research has been done in the field of water quality in the coastal waters in this region and, in general, other parts of Indonesian waters (Dekker et al., 1999; Van der Woerd & Pasterkamp, 2001; Hendiarti et al., 2004).

Ocean color applications utilize the spectral characteristics and variations of radiometric data to derive information about some of the constituents of the water. Techniques for water constituent retrieval have evolved from an empirical to the semi-analytical approach. The empirical algorithms (Gordon & Morel, 1983) often focus on a single constituent concentration. The semi-analytical method is capable of retrieving three water constituents simultaneously. This model has potential of providing accurate retrievals of several parameters because they attempt to model the physics of ocean color (Maritorena et al., 2002). Semi-analytical models have been developed to derive waters constituents such as chlorophyll a (Chl a) concentration, total suspended matter (TSM) concentration, and colored dissolved organic matter (CDOM) absorption (D'Sa et al., 2002; Maritorena et al., 2002; Haltrin & Arnone, 2003; Doerffer & Schiller, 2007; Van der Woerd & Pasterkamp, 2001; Le et al., 2009; Salama & Stein, 2009; Salama et al., 2009; Salama & Shen, 2010a).

Understanding bio-optical properties of coastal waters is a key issue to improve the accuracy of derived water constituents from ocean color data (e.g., Babin et al., 2003; Hamre et al., 2003). Various studies in coastal waters have demonstrated the need for regional algorithms to obtain better estimation of water constituents (Kahru & Mitchell, 2001; Reynolds et al., 2001; D'Sa et al., 2002). Inherent optical properties (IOP) are the optical properties of water that are independent of the ambient light field (Preisendorfer, 1976). IOP include light absorption and scattering coefficients. The apparent optical properties (AOP) as measured by a spectroradiometer are additionally dependent on the ambient light field and its geometric structure. Various models have been developed to relate IOP to AOP (Gordon et al.,

1975; Morel & Prieur, 1977; Gordon & Morel, 1983; Kirk, 1984; Gordon, 1991; Carder et al., 1999; Stramski et al., 2002; IOCCG, 2006). Salama et al. (2009) developed an algorithm, modified from the GSM semi-analytical model, for deriving bio-optical properties such as IOP in inland waters. The model appears promising for these turbid coastal waters.

Subsurface irradiance reflectance, $R(0-)$ is an AOP given by Gordon et al. (1975) as a function that relates upwelling irradiance (E_u) to downwelling sun irradiance (E_d) at null depth. The model of direct interest to this study is an inversion of a semi-analytical model from $R(0-)$ into IOPs and specific inherent optical properties (SIOP). SIOP can be estimated from derived values of IOP and measured concentrations of water constituents. Until recently, most of the IOP or SIOP data were collected from European coastal waters, mainly at mid-latitude, e.g., the North Sea and Baltic Sea. Limited research on the variability of IOP and associated SIOP values has been carried out in the tropical equatorial region, especially in Indonesian waters. The objectives of this study are to estimate the SIOP of the Berau estuarine water using ocean color data, model inversion, and in situ measurements and to estimate the TSM and Chl a concentration from MERIS satellite sensor data using a semi-analytical model.

Materials and methods

Study area

The Berau estuary is a semi-enclosed coastal water body situated in East Kalimantan Province, Indonesia, located between 88 01°45′ and 02°35′ North and 117°20′ and 118°45′ East (Fig. 1). Shallow marine environments in this system range from turbid coastal and estuarine waters through inner reef to open oceanic and shelf-edge reef conditions, and provide an interesting opportunity to study coastal dynamics.

The Berau barrier reef is a large flourishing delta-front barrier reef located about 40 km from the mouth of the Berau River, with numerous patch and platform reefs, such as Derawan Island. The sediment plumes from the Berau River affect the west side of the barrier reef that is closer to the river mouth. Increased sediment fluxes may also affect coral reef life in this area. Water quality monitoring in the
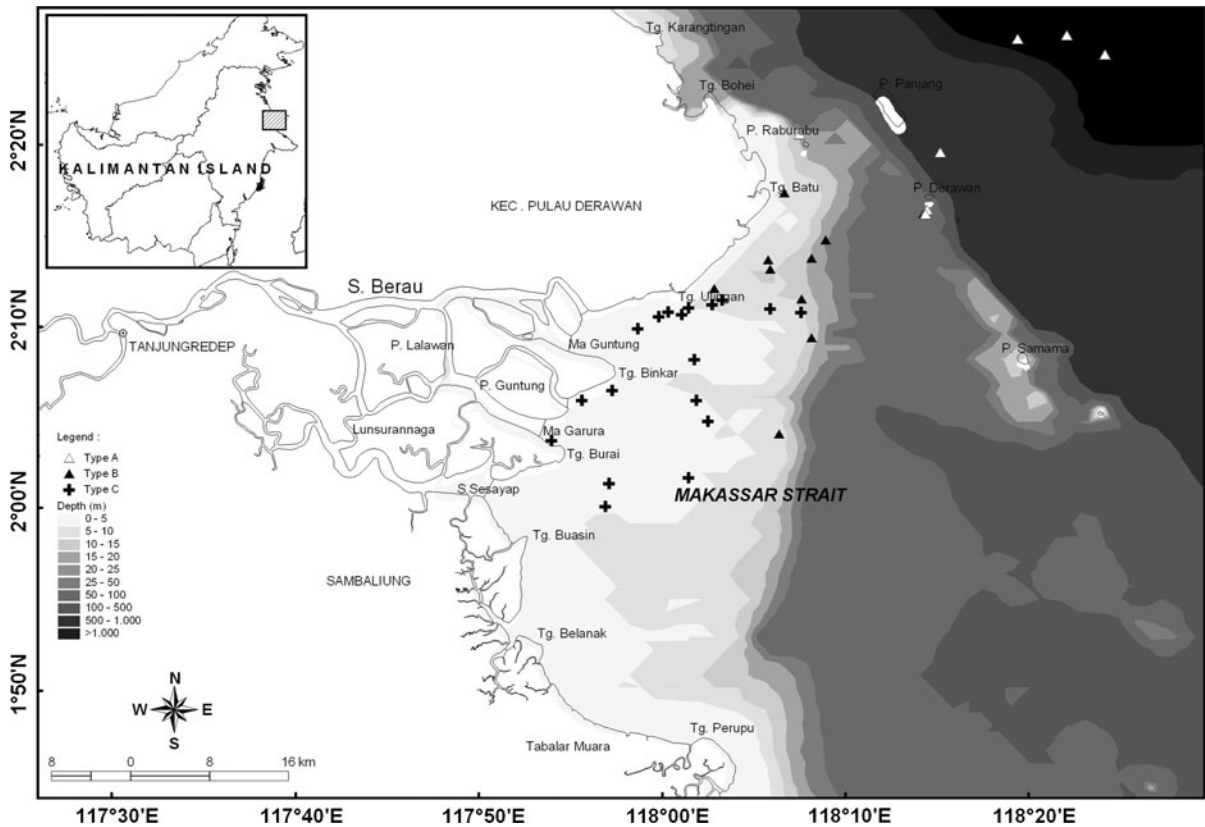
Fig. 1 The study area and field station locations in the Berau estuary, East Kalimantan Province, Indonesia (*source*: Topographical Map). The stations are located in different types of waters as shown by the *different symbols*

Berau estuary is therefore an essential part for the protection of these aquatic systems.

In situ constituent measurements and classification of coastal waters

In situ water quality data were collected in the Berau estuary during the 2007 dry season, from 27 August to 18 September 2007, at representative locations (shown in triangle symbols on Fig. 1) ranging from more than 100 m depth in clear open-ocean waters to less than 2 m depth in very turbid coastal waters. The water samples were collected at depth between 20 and 50 cm and were analyzed for their content of total suspended matter TSM and Chl *a*. The REVAMP or regional validation of MERIS chlorophyll products' protocol was used in the analysis (Tilstone et al., 2002). Other water quality variables as Secchi disc depth, EC, temperature, pH, turbidity,

dissolved oxygen, and salinity were also measured at the locations using a Lamotte Secchi disk and a Horiba U10 water quality multiprobe.

In January 2009, a small additional field campaign was carried out in the Berau Estuary. The main parameter collected then was colored dissolved organic matter or CDOM absorption (a_{CDOM}). The water samples collected in the field were filtered using a Whatman 0.22-μm filter following REVAMP protocols (Tilstone et al., 2002), and the CDOM absorption spectra were measured in the laboratory using an Ocean Optics spectrometer.

An exploratory multivariate analysis was initially performed on the in situ data set to infer variations and possible interdependencies or relationships among the measured variables. An unsupervised K-means clustering method was applied using Chl *a*, total suspended matter (TSM) in combination with Secchi disk depths.

In situ optical measurements and spectral data analysis

At the same locations of the in situ measurements, under and above water radiometric measurements were carried out using an Ocean Optic Spectrometer USB4000 following REVAMP protocols (Tilstone et al., 2002). Spectra of subsurface irradiance were measured at three water depths of, respectively, 10, 30, and 50 cm. Subsurface irradiance reflectance $R(0-)$ was calculated from the measured subsurface irradiance spectra at 10, 30, and 50 cm depth. Above water radiometric observations consisted of measurement of sky irradiance and water leaving reflectance. The optical data were analyzed using a hydro-optical modeling approach.

Hydro-optical model

Hydro-optical models relate measured radiometric quantities above the water surface to the IOP of the water's upper layer, hence constituent concentrations. In the absence of IOP measurements, we chose a subsurface irradiance reflectance model (Gordon et al., 1975) for estimating IOP and associate SIOP using in situ measurements of under and above water reflectances as AOP and an inversion method as explained hereafter.

Subsurface irradiance reflectance, $R(0-)$, is the ratio of upward (E_u^-) and downward irradiance (E_d^-) just beneath the water surface and was calculated as (de Haan et al., 1999):

$$R(\lambda, 0^-) = \frac{E_u^-}{(1 - r_\Theta(1 - F) - r_{dif}F)E_d^+ + 0.48E_u^-}. \tag{1}$$

The E_d^+ and E_u^- are, respectively, the down-welling irradiance just above the water surface and the upwelling irradiance just beneath the water surface. These radiometric quantities (E_d^+ and E_u^-) were measured during the field campaign as explained in "Hydro-optical model" section. The Fresnel reflectance coefficient for sunlight, r_Θ, was calculated from viewing illumination geometry. F is the fraction of diffuse light of E_d^+. The Fresnel reflectance coefficient of diffuse light (r_{dif}), in this study was set to 0.06 (Jerlov, 1976).

Subsurface irradiance reflectance in Eq. 1 can be related to the IOP of the water using the Gordon et al. (1975) model:

$$R(\lambda, 0^-) = f\frac{b_b(\lambda)}{a(\lambda) + b_b(\lambda)}, \tag{2}$$

where f is a proportionality factor which can be treated as a constant with a default value of 0.33 (Gordon et al., 1975); $a(\lambda)$ and $b_b(\lambda)$ are the bulk absorption and backscattering coefficients. We will use the collective term IOP to refer to absorption and backscattering coefficients.

The absorption $a(\lambda)$ and backscattering $b_b(\lambda)$ coefficients (Eq. 2) are the sum of contributions by the various seawater constituents. These IOP are separated into components such as the dissolved and particulate fractions and water. The total absorption coefficient a (m^{-1}) is the sum of the contributions by pure water (a_w), phytoplankton, detritus or non-algal particles, and CDOM absorption. The total backscattering coefficient $b_b(\lambda)$ can be separated into contribution of pure water and total suspended matter (TSM). IOPs can be related to constituent concentrations and their SIOP as follows (Gege, 2005):

$$a(\lambda) = a_w(\lambda) + C_{chl} \cdot a_{chl}^*(\lambda) + X \cdot a_x^*(\lambda) + Y \cdot a_y^*(\lambda), \tag{3}$$

$$b_b(\lambda) = b_{b,w}(\lambda) + C_s \cdot b_{b,TSM}^*(\lambda), \tag{4}$$

where C_{chl}, X, Y, indicate the concentrations of Chl a, non-algae particles, and gelbstoff, respectively. SIOPs of these constituents are denoted as a_{chl}^*, a_x^*, and a_y^*, respectively. Absorption and scattering of water molecules, $a_w(\lambda)$ and $b_{b,w}(\lambda)$, were taken from Pope & Fry (1997) and Morel (1974), respectively. $b_{b,TSM}^*(\lambda)$ is the specific backscattering coefficient of total suspended matter.

Measured radiometric quantities in the field ("Hydro-optical model" section) can now be related to the IOP of the water upper layer using Eqs. 1 and 2. Equation 2 is then inverted to derive the IOP of the water upper layer. The SIOP a_{Chl}^* and $b_{b,TSM}^*$ of the Berau estuary are estimated from the derived IOP and measured concentrations as:

$$b_{b,TSM}^*(\lambda) = b_{b,TSM}/C_{TSM} \tag{5}$$

$$a_{Chl}^*(\lambda) = a_{chl}/C_{chl}. \tag{6}$$

Light absorption by CDOM also constitutes an important light interaction in water, responsible for altering the under water light field significantly. Absorption by yellow substances is the product of dissolved organic matter concentration and its specific absorption. The following exponential approximation (Bricaud et al., 1981) was used to characterize CDOM absorption in water:

$$a_{CDOM}(\lambda) = a_{CDOM440}\, e^{-[S(\lambda - \lambda 0)]}, \tag{7}$$

where $a_{CDOM}(\lambda)$ is the light absorption by CDOM in (m^{-1}), λ_0 is a reference wavelength in (nm), and S denotes the spectral slope of the absorption curve with unit (nm^{-1}). Commonly used standard values for the slope and reference wavelength are $\lambda_0 = 440$ nm and $S = 0.014$ nm^{-1} (Bricaud et al., 1981).

Analysis of satellite ocean color data

Medium Resolution Imaging Spectrometer (MERIS) Level 1b of Reduced Resolution (RR) and Full Resolution (FR) satellite image data were used in this study. The satellite data were acquired from the European Space Agency (ESA) under a principal investigator contract. Among the several satellite data available, there was only one MERIS data which a full match-up in time with the in situ measurement, namely on 31 August 2007. This data were used to analyze the match-up of satellite retrieval of optical properties and water quality constituent with in situ observations.

The MERIS Reduced Resolution (RR) Level 1 satellite image of 31 August 2007 was used in this stage. Atmospheric correction was carried out using the method of Gordon & Wang (1994). The look-up table for atmospheric path radiances was generated using the 6S model (Vermote et al., 1997). The distinctive signal of turbid waters was accounted for in the computations using the method of Salama & Shen (2010b). IOPs were derived from MERIS water leaving reflectances using the model of Salama et al. (2009). The statistical evaluation of $R(0-)$, IOP, and SIOPs as well as TSM and Chl a concentrations were done by evaluating the coefficient of determination (R^2) and Root Mean Square Error (RMSE). A logarithmic scale was used in the analysis of RMSE following standard practice (IOCCG, 2006, Eq. 2.1, pp. 18).

Results

Turbidity-based classification of coastal waters

The in situ measurements were submitted to an exploratory statistical multivariate analysis. The application of a K-means clustering analysis on measured concentrations of Chl a, TSM and Secchi disk depth resulted in a grouping of the data into three distinct classes or water types. Figure 2 shows the mean and standard deviation values of Chl a and TSM concentrations as well as the Secchi disc depth for the three groups. Water types A, B, and C correspond,
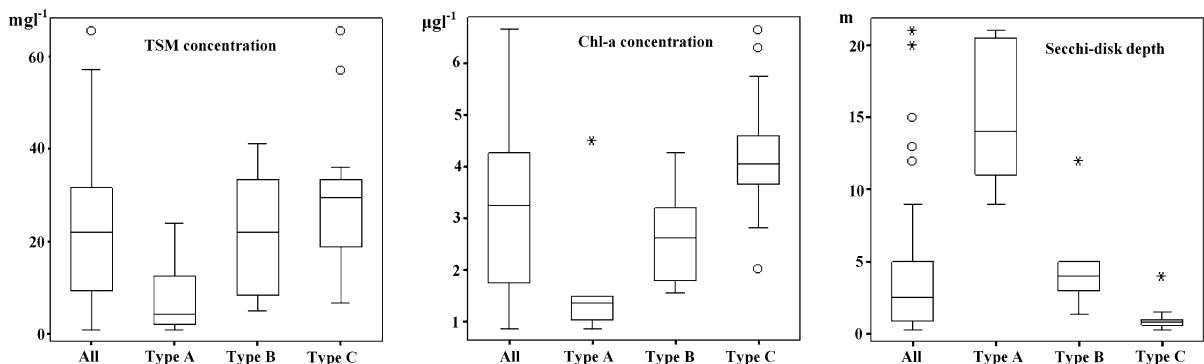

Fig. 2 Box plot of the TSM, Chl a, and Secchi disc depth for all in situ data plotted per water types A, B and C. *Boxes* indicate the variations as defined by the standard deviation; the median is indicated as horizontal line in the box; Quartile 1 and Quartile 3 indicate minimum and maximum value respectively; *circle* indicates outlier value and *star* indicates extreme value
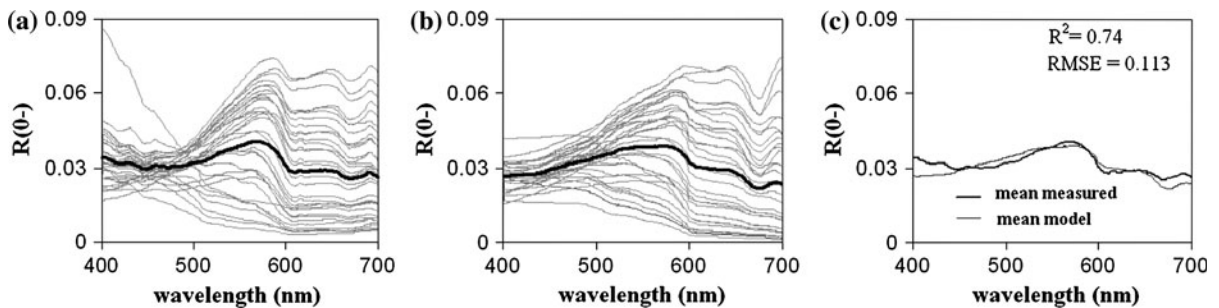
Fig. 3 Subsurface irradiance reflectance $R(0-)$ field measurements: **a** measured $R(0-)$; **b** modeled best fits to measured; **c** comparison of means (no. of spectra = 36). *Thick lines* indicate the mean of the data

respectively, to low, moderate, and high concentrations of Chl *a* and total suspended matter (TSM). With respect of location, they correspond to offshore and shelf edge, transitional region, and near shore coastal waters. This unsupervised classification based on measured water quality properties was subsequently confronted with the spectral signatures and optical properties of the waters, derived from the spectral measurements and data analysis as detailed hereafter.

Subsurface irradiance reflectance of in situ measurements

The subsurface irradiance reflectance $R(0-)$ is an AOP and was computed from the measured irradiances using Eq. 1, and the resulting 36 spectra are presented in Fig. 3a. Model (Eq. 2) best-fits to the measured spectra are shown in Fig. 3b. The means of measured $R(0-)$ and the model best-fit are compared in Fig. 3c. There is a good agreement between measured and model best-fit spectra with a $R^2 = 0.74$ and RMSE values of 0.113. Some mismatch is apparent in the short (blue) and near infrared (NIR) wavelengths.

The reflectance spectra were then clustered among the sampling points of three water turbidity types as shown in Fig. 4a–c. Their mean values are displayed in Fig. 4d, e, and f for water types A, B, and C, respectively. In Fig. 4a, the $R(0-)$ of Type A water shows an $R(0-)$ curve shape different from that of the other two water types. The subsurface irradiance reflectance of this water type has the highest value in the short wavelength (blue) and continuously decreases with increasing wavelength. A cross-check with the Secchi disc depth data indicates that this type of water corresponds mostly to clear blue water. Figure 4b shows the $R(0-)$ of Type B water. The

curves show a wide stable range between 400 and 580 nm. A first moderate peak is obtained between 550 and 580 nm. The second peak is found at around 685 nm. A cross-check with the Secchi disc depth data indicates that this type of water signature corresponds mainly to the moderately turbid waters in the study area. Figure 4c shows the irradiance reflectance of Type C water. With the exception of the peak at 400 nm, this generally has the highest peak among the water types. The first peak shifts toward 560–580 nm. The second peak occurs at 685 nm. Reference to the Secchi disc depth data indicates that this type of water corresponds mainly to the most turbid waters in the study area.

A statistical analysis of $R(0-)$ measured and $R(0-)$ modeled of 36 locations are plotted in Table 1. The R^2 of all wavelengths on three types of water are high, especially for Types B and C waters. Based on the values of R^2 (high) and RMSE (low), it can be concluded that at the wavelength of 489, 509, 559 nm and 619 nm, the best match between measured and modeled $R(0-)$ are achieved. After data classification, the R^2 improved significantly. However, the RMSE of the classified data sets was higher, particularly for Type A water. A closer inspection of the statistical values indicates that the result of fitting between measured and modeled $R(0-)$ in Type A waters (clear water) is generally less well matched than the results obtained for the other water types. The fitting of measured and modeled $R(0-)$ in Types B and C waters gives sufficiently good results.

Inherent optical properties (IOP)

The IOP of the coastal waters were derived using inversion of the hydro-optical model (Eq. 2). The
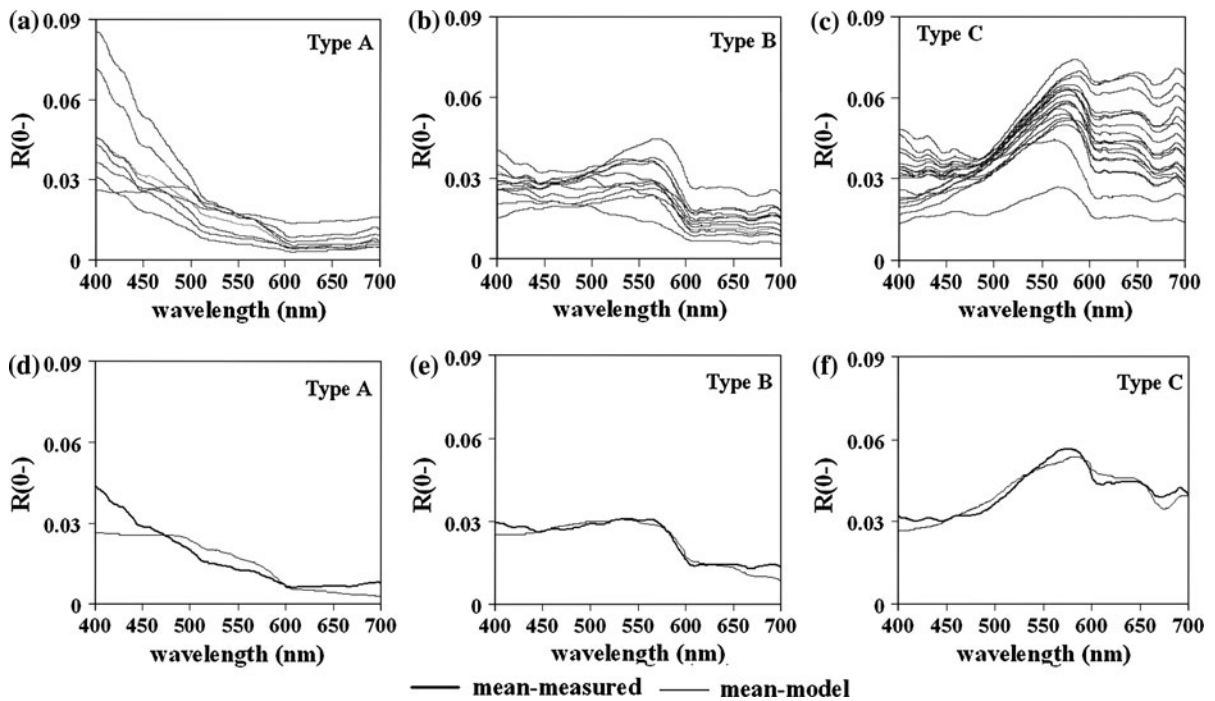
Fig. 4 $R(0-)$ spectra of in situ measurements for the three water types: **a** Type A water ($n = 8$), **b** Type B water ($n = 10$), and **c** Type C water ($n = 18$). The mean of $R(0-)$ in situ measurement thick line) and mean of $R(0-)$ derived from inversion model (*thin line*) are shown in **d** Type A water, **e** Type B water and **f** Type C water

Table 1 Correlation statistics between measured and modeled subsurface irradiance reflectance $R(0-)$ for the three water types and selected MERIS sensor channel wavelengths

λ (nm)	RMSE			R^2			Slope			Intercept		
	Type A	Type B	Type C	Type A	Type B	Type C	Type A	Type B	Type C	Type A	Type B	Type C
412	0.175	0.057	0.057	0.83	0.87	0.93	0.415	0.740	0.646	0.010	0.004	0.007
442	0.083	0.013	0.018	0.92	0.96	0.98	0.641	0.986	0.870	0.006	0.000	0.003
489	0.064	0.028	0.036	0.97	0.95	0.92	1.063	0.963	1.188	0.002	0.003	0.004
509	0.133	0.019	0.027	0.85	0.99	0.96	1.046	1.026	1.101	0.004	0.000	0.002
559	0.155	0.017	0.027	0.77	1.00	0.99	0.942	0.932	0.917	0.005	0.001	0.001
619	0.136	0.075	0.028	0.56	0.99	1.00	0.513	1.215	1.022	0.002	0.003	0.002
664	0.284	0.138	0.032	0.57	0.99	1.00	0.351	1.044	0.993	0.001	0.003	0.002
680	0.362	0.187	0.066	0.56	0.99	0.99	0.331	0.964	0.947	0.001	0.003	0.003
708	0.531	0.248	0.070	0.47	0.96	0.96	0.233	0.852	1.171	0.001	0.003	0.007

backscattering coefficient of total suspended matter (TSM) at 550 nm ($b_{b,TSM}$) and the absorption coefficient of Chl a at 440 nm (a_{Chl}) were derived from in situ optical measurements using Eqs. 2, 5, and 6, and presented in Table 2. The mean of $b_{b,TSM}$ data shows a higher value for Type C water (0.604 m^{-1}) than for Type A (0.019 m^{-1}) or Type B (0.196 m^{-1}) waters.

The absorption of Chl a shows a similar trend with the backscattering coefficient and increased from Types A to C waters.

The CDOM absorption coefficient at 440 nm ($a_{CDOM440}$) and the spectral slope S of the absorption line was measured on six water samples taken at six locations (see Fig. 1) in January 2009 between lower

Table 2 Descriptive statistics of inherent optical properties (IOP) $b_{b,TSM}$ in (m^{-1}) at 550 nm, and a_{Chl} in (m^{-1}) at 440 nm for the three water types (A, B, C) in the Berau estuary observed in August and September 2007

	$b_{b,TSM}$ (m^{-1})			a_{Chl} (m^{-1})		
	Type A	Type B	Type C	Type A	Type B	Type C
Mean	0.019	0.196	0.604	0.037	0.057	0.108
Minimum	0.010	0.033	0.180	0.023	0.028	0.043
Maximum	0.036	0.527	0.995	0.061	0.110	0.484
SD	0.009	0.174	0.247	0.011	0.028	0.098

left (2°11′05″N; 117°43′36″E) and upper right (2°14′50″N; 118°11′40″E). Table 3 shows the resulting statistics of the spectral slope S and CDOM absorption coefficient a_{CDOM}, permitting to quantify light absorption by CDOM in the Berau coastal waters using Eq. 7. The a_{CDOM} was higher in the Berau river (mean = 1.35 m^{-1}) and logically decreased toward the open sea (mean = 0.19 m^{-1}). The a_{CDOM} around the Berau river mouth was 0.473 m^{-1}. The spectral slope S in the open sea waters was lower (0.011 nm^{-1}) than in the Berau river mouth water (0.013 nm^{-1}).

Specific inherent optical properties (SIOP)

The derived values of the TSM specific backscattering coefficient are given in Table 4. The $b_{b,TSM}^{*}$ is 0.020 m^2 g^{-1} in turbid water (Type C) and 0.003 m^2 g^{-1} in open sea (Type A). The values are increasing form clear water to turbid water, corresponding to off shore and near shore sites.

The specific absorption coefficients of Chl a are given in Table 5. In the Berau estuary waters, the values of a_{Chl}^{*} were comparable for the three types of waters. The values seem slightly increasing from Type C (0.021 m^2 mg^{-1}) and Type B (0.020 m^2 mg^{-1}) to Type A (0.027 m^2 mg^{-1}) waters. In the case of a_{Chl}^{*},

Table 3 Descriptive statistics of the colored dissolved organic matter (CDOM) light absorption measured at 440 nm and spectral slope exponent (S) sampled in the January 2009 field campaign (SD is standard deviation)

Parameters	Min	Max	Mean	SD
$a_{CDOM440}$ (m^{-1})	0.140	1.666	0.672	0.583
Spectral slope S (nm^{-1})	0.015	0.011	0.012	0.002

Table 4 Specific backscattering coefficient of TSM, $b_{b,TSM}^{*}$ (m^2 g^{-1}), at 550 nm for all sample points and water types

Water type	Known		Derived		RE (%)
	Station	$b_{b,TSM}^{*}$	Station	$b_{b,TSM}^{*}$	
Type A	30-2	0.005	5-6	0.008	36
	31-1	0.004	5-7	0.005	3
	3-1	0.003	15-3	0.002	19
	5-1	0.002	15-4	0.002	21
	Mean	0.003		0.004	20
Type B	1-8	0.004	11-3	0.003	44
	3-4	0.009	1-9	0.007	42
	8-10	0.008	18-6	0.009	11
	13-6	0.019	18-5	0.017	10
	15-7	0.015	16-3	0.012	30
	Mean	0.011		0.009	27
Type C	11-4	0.022	11-6	0.016	40
	11-7	0.021	8-3	0.023	8
	8-4	0.027	8-6	0.027	1
	8-7	0.015	8-9	0.012	33
	1-6	0.019	7-10	0.018	4
	1-7	0.021	16-10	0.023	9
	17-9	0.012	18-10	0.016	23
	17-10	0.020	18-9	0.028	26
	29-1	0.027	29-7	0.021	25
	Mean	0.020		0.020	19

the relative error is 5% for Type A, 11% for Type B, and 10% for Type C water (Table 5).

The result of the simulations to assess the difference between derived and modeled $b_{b,TSM}^{*}$ and a_{Chl}^{*} is plotted in Fig. 5. It shows the correlation between the derived and modeled values of SIOP for $b_{b,TSM}^{*}$ and a_{Chl}^{*}. The R^2 of $b_{b,TSM}^{*}$ is 0.87 and the R^2 of a_{Chl}^{*} is 0.89. From the performance of $b_{b,TSM}^{*}$, it can be concluded that a high correlation between the modeled data and the derived data set can be observed. The RMSE was lower for the $b_{b,TSM}^{*}$ when compared to the error on a_{Chl}^{*}.

Satellite ocean color imagery and in situ match-up

A statistical analysis of the TSM and Chl a concentration estimated from MERIS observations and matching in situ measurements is given in Fig. 6 and Table 6. In general, there is a good agreement between TSM estimated from MERIS and TSM

Table 5 Specific Chl a absorption, a_{Chl}^* (m^2 mg^{-1}), at 440 nm for all sample points and water types

Water type	Calibration		Derived		RE (%)
	Station	a_{Chl}^*	Station	a_{Chl}^*	
Type A	30-02	0.031	5-1	0.031	1
	31-01	0.012	15-05	0.013	10
	3-1	0.026	15-04	0.027	2
	5-6	0.041	15-03	0.043	4
	Mean	0.027		0.028	5
Type B	1-8	0.032	11-3	0.028	14
	1-9	0.011	13-6	0.010	4
	3-4	0.026	8-10	0.027	5
	18-4	0.021	18-5	0.022	4
	5-7	0.010	16-4	0.009	11
	Mean	0.02		0.019	8
Type C	11-4	0.017	11-7	0.016	8
	11-6	0.038	17-09	0.041	8
	8-3	0.021	8-7	0.020	1
	8-4	0.035	8-6	0.031	10
	8-9	0.017	7-6	0.015	13
	7-10	0.020	18-06	0.023	16
	1-7	0.012	17-10	0.013	16
	16-10	0.016	18-10	0.017	5
	29-07	0.015	29-1	0.017	10
	Mean	0.021		0.022	10

Table 6 Correlation statistics between measured TSM and Chl a concentrations and MERIS satellite sensor estimates for the three water types

	TSM concentration			Chl a concentration		
	Type A	Type B	Type C	Type A	Type B	Type C
R^2	0.89	0.96	0.66	0.62	0.70	0.64
RMSE	0.079	0.060	0.465	0.528	0.206	0.177
Slope	0.630	0.856	0.386	1.806	0.875	0.488
Intercept	0.206	−1.106	−0.716	−1.379	−0.029	3.829
N	8	10	18	8	10	18

measured in Types A and B waters. The R^2 values are 0.89 or higher with a RMSE less than 0.060 mg l^{-1}. On the other hand, derived values of TSM seem less reliable for Type C water with $R^2 \sim 0.66$ and RMSE value up to 0.47 g l^{-1}. In the case of Chl a concentration, there is a moderately good correlation between the estimated and measured values for all types of waters. The R^2 values are between 0.62 and

0.7. The values of RMSE are, however, in opposite to those obtained for TSM, i.e., larger errors are obtained in clear, Type A, water with RSME value of 0.528 μg l^{-1} which is threefold larger than that of Type C waters. For both variables, TSM and Chl a, the best match-up results were obtained for Type B waters. This water type showed a large R^2 (≥ 0.7), a near to unity slope (~ 0.9) and small RMSE values of 0.06 mg l^{-1} and 0.21 μg l^{-1} for TSM and Chl a, respectively.

Figure 7a and b illustrates the estimated TSM and Chl a concentrations for the Berau estuary waters from full resolution MERIS data on 17 May 2007. The 300-m resolution of MERIS data reveals the spatial distribution of TSM concentration and Chl a throughout the study area. The gradients of TSM concentrations are particularly evident in the middle section of the image where the Berau river flows into the estuary.

Discussion

Classification of coastal waters

Both the multivariate clustering analysis on in situ measured water quality variables and the corresponding in situ measured spectral signatures and optical properties permitted to distinguish three water types in the coastal zone around the Berau estuary. Type A water represents clear optically deep waters, close to the open ocean and shelf edge. This water type is characterized by low TSM concentration (mean = 8 mg l^{-1}), low Chl a concentration (mean = 1.65 μg l^{-1}), and high Secchi disc depths (mean = 15 m). Type B water represents the region of fresh water influence where the fresh water meets saline seawater. This water type is characterized by TSM concentration around 20.14 mg l^{-1}, Chl a concentration 3.19 μg l^{-1} and Secchi disc depth around 4.5 m. Hundreds of typical in-water bamboo fishing houses are located in this Type B water. The last, Type C water is located around Berau river mouth with the TSM concentrations higher compared to others (mean = 28.9 mg l^{-1}) as well as high Chl a concentrations (mean = 4.43 μg l^{-1}) and low Secchi disc depths (mean = 1 m). Also the IOPs of Type C water are higher than those of the other two water types. Similar results of decreasing IOP values moving off-shore were

Fig. 5 Scatter plot of model versus derived SIOPs: **a** specific backscattering coefficient of TSM, $b^*_{b,TSM}$, at 550 nm and **b** specific absorption coefficient of Chlorophyl, a^*_{Chl}, at 440 nm
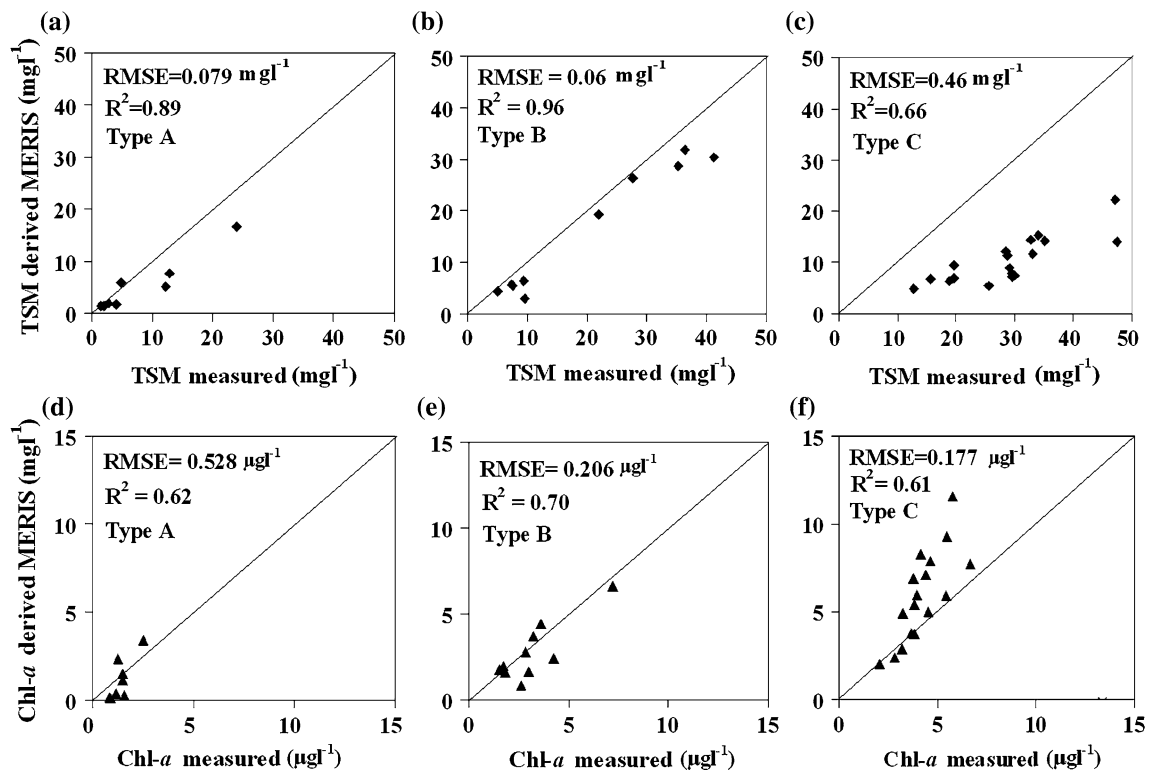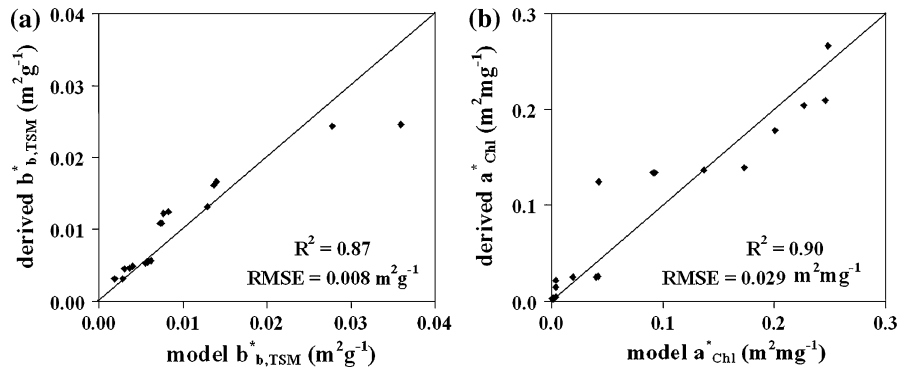

Fig. 6 Scatter plot of the in situ measured TSM and Chl a versus MERIS satellite sensor estimated TSM and Chl a for the three water types A, B, and C

reported for the North Sea waters (Salama et al., 2004; Astoreca et al., 2006).

Specific backscattering of TSM, $b^*_{b,TSM}$

The derived values of specific backscattering coefficient of total suspended matter (b^*_{TSM}, TSM) in the Berau estuary vary about an order of magnitude between Types A and C water, with the highest values being measured in turbid waters. In general, derived values of b^*_{TSM} water are in the range found by previous studies. For example, Dekker (1993) found a specific scattering coefficient (b^*_{TSM}) of 0.23–0.79 m^2 g^{-1} for different trophic states in lakes, with a backscattering to scattering ratio varying from 0.011 to 0.020 m^2 g^{-1} and a backscattering

coefficient of TSM ($b_{b,TSM}^*$) of 0.003–0.016 m^2 g^{-1}. Ibelings et al. (2001) reported a specific scattering coefficient of 0.25–0.31 m^2 g^{-1} for Lake IJssel in the Netherlands, with a backscattering to scattering ratio of 0.035–0.045 and a backscattering coefficient of TSM ($b_{b,TSM}^*$) of 0.009 to 0.014 m^2 g^{-1}. However, our result seems to be higher than the results found by Heege (2000, in Albert & Mobley, 2003), who investigated the scattering of suspended matter in lake Constance. He found the specific scattering and backscattering coefficient of TSM to be $b_{TSM}^* = 0.45$ m^2 g^{-1} and $b_{b,TSM}^* = 0.009$ m^2 g^{-1}, and thus a scattering ratio of 0.019. Table 4 shows that the relative error of $b_{b,TSM}^*$ at each station is relatively high, with an error average of 20% for Type A, 27% for Type B, and 19% for Type C water. Although the individual errors between known data sets and derived data sets are high, the aggregate value of relative error for each type of water can be considered satisfactory. This discrepancy between derived $b_{b,TSM}^*$ in the Berau and reported values elsewhere is expected and can be probably explained by differences in sediment characteristics, i.e., particle size and composition. For example, Stramski et al. (2002) and Babin et al. (2004) showed that very fine particles are a more efficient scatterer and absorber of light than coarse particles.

Specific absorption of phytoplankton, a_{Chl}^*

Although the specific absorption coefficient of phytoplankton can vary for the same region (Mitchell & Kiefer, 1988), the Berau estuary waters showed almost a constant value. Its value (0.019–0.027 m^2 mg^{-1}) is similar to what has been reported elsewhere. For example, Prieur & Sathyendranath (1981), Sathyendranath et al. (1987), and Gallegos & Correl (1990) found that a_{Chl}^* for oceanic and coastal waters varies from 0.01 to 0.047 m^2 mg^{-1}, whereas Smith & Baker (1981) found that a_{Chl}^* varied between 0.039 and 0.168 m^2 mg^{-1}. On the other hand, Heege (2000, in Albert & Mobley, 2003) and Le et al. (2009) measured mean values of 0.034 m^2 mg^{-1} for Lake Constance and Lake Taihu in China, respectively.

Derived values of Chl a absorption a_{Chl} at 440 nm (m^{-1}) indicate that the Berau estuary has a lower content of green pigment when compared to other regions. For example, Astoreca et al. (2006) reported a_{Chl} values of the North Sea coastal waters to

be between 0.48 ± 0.63 m^{-1} in May 2004 and 0.21 ± 0.14 m^{-1} in July 2004 which are four times larger than derived values in Type C waters of the Berau estuary (see Table 3). On the other hand, offshore waters of the Berau and North Sea have comparable values of a_{Chl}. Astoreca et al. (2006) reported for offshore water of the North Sea, a_{Chl} values of 0.08 ± 0.04 m^{-1} in May 2004 and 0.05 ± 0.03 m^{-1} in July 2004, which compare to Types A and B waters of the Berau with mean values of 0.037–0.057 m^{-1}, respectively (see Table 3). These results indicate that the Berau estuarine waters have a relative low trophic state. This could also indicate that the average cell size of phytoplankton in the Berau estuary is small which is a characteristic of oligotrophic waters (Mercado et al., 2007).

Colored dissolved organic matter (CDOM)

The values of the CDOM absorption coefficient in the Berau estuary ranged from 1.67 m^{-1} in the river to 0.091 m^{-1} in clear open seawater. At the Berau river mouth, the CDOM absorption value was 0.5 m^{-1}. It is worth noting that the lowest measured values of CDOM absorption in the Berau are still higher than the threshold for Case-2 waters of ~ 0.03 m^{-1} (Kratzer et al., 2008). The relatively high values of CDOM absorption can also be noticed from the lower reflectance values of the Type C waters in the Berau estuary as shown in Fig. 4c. The spectral slope exponent of the CDOM absorption curve was found to be spatially homogenous and in the range 0.011–0.015 nm^{-1} with an average of 0.012 ± 0.002 nm^{-1}.

MERIS satellite image and in situ data match-up

A good fit was found between MERIS-derived and in situ measured variables of TSM and Chl a concentrations. For the comparison, we used the statistical parameters R^2, RMSE, slope, and intercept. The best results were obtained for the moderately turbid waters of Type B. This can be explained by several reasons: (i) a large error is induced by atmospheric correction in cloud-shadowed (Matthew et al., 2000) and hazy regions which prevail offshore the Berau estuary; (ii) relatively large errors are induced by model parameterization and inversion in turbid waters; (iii) an error can be induced by model parameterization and inversion in clear water areas affected by bottom reflectance.
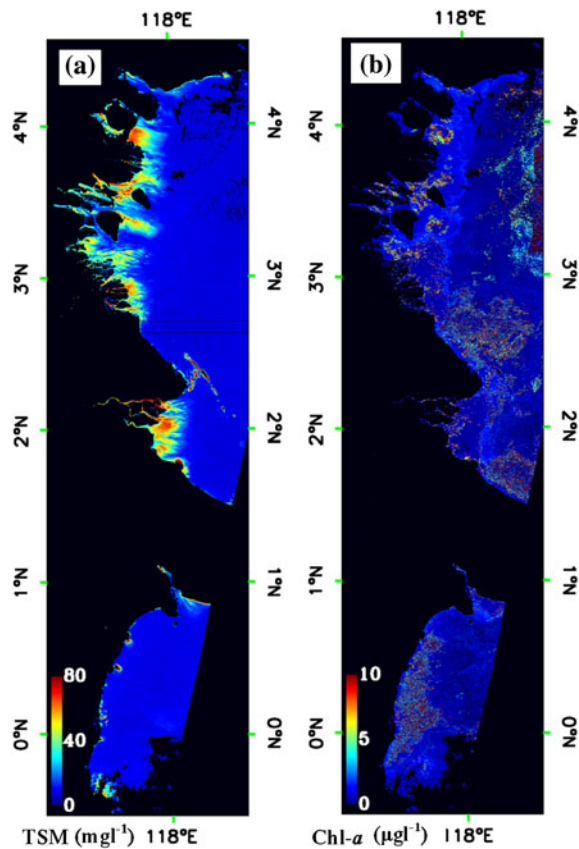
Fig. 7 TSM map (**a**) and Chl *a* map (**b**) derived from the MERIS Full Resolution Level 1b image of 17 May 2007

The relative contribution of these different error components to the total uncertainty in derived IOP was estimated for the same model as used in this study and MERIS sensor to be about 46–50% for atmosphere correction, 40–45% for model parameterization-inversion, and 5–13% for sensor noise (Salama & Stein, 2009).

The spatial distribution of TSM and Chl *a* concentrations

The concentrations of TSM and Chl *a* were derived from the MERIS image using estimated values of the SIOP. The results in Fig. 7 show that TSM concentrations are higher in coastal waters and decrease toward the open ocean. However, the distribution of MERIS-derived Chl *a* concentrations presents a linguiform-like belt situated outside of the turbidity zone (TSM < 50 mg l^{-1}) of TSM. This belt-shape of Chl *a* concentrations can be explained by the low

concentrations of TSM outside the turbidity zone and increased level of nutrients transported by the Berau river plume which creates optimal conditions for phytoplankton flourishing if supply of light energy is enough. This belt, of increased Chl *a* concentration, is followed by a decrease of phytoplankton biomass due to a decrease in nutrient levels and an increase in salt content.

Uncertainties

The SIOP were derived from in situ measurements and model inversion. Each step of the derivation procedure has an error component which contributes to the total uncertainty of the derived SIOP. The total uncertainty of derived SIOP is a lumped effect of several error components, namely measurement, model parameterization and inversion, and atmospheric correction.

Field radiometric measurement

In situ data may contain significant errors caused by environmental factors, instrumental shortcomings, and human errors (Hooker & Maritorena, 2000; Chang et al., 2003). In this study, we observed that the subsurface irradiance reflectance $R(0-)$ in the Berau estuary varied strongly from clear water to turbid waters due to the different water constituents. In general, it can be observed that the modeled $R(0-)$ has good agreement with the $R(0-)$ measurements. However, matching was poorer for some locations, particularly in the clear deeper waters rather than the shallow turbid waters. This tendency of decreasing measurement reliability in clear water can be attributed to the reduced signal-to-noise ratio of the used Ocean Optics device in very clear water under cloud and atmospheric haze cover: (i) the almost persistence of clouds over the region during field measurements influenced the sun irradiation and light field; (ii) also very clear waters reduce the signal of the water leaving reflectance, due to reduced backscattering.

Model parameterization and inversion

The second major source of uncertainty is due to model parameterization. The model used here: (i) ignores the differences in phytoplankton species

that may co-exist in coastal waters; (ii) ignores the large inherent variability of Chl a absorption as measured in nature; and (iii) combines the absorption effect of detritus and CDOM in one spectral shape and magnitude. Inversion uncertainty is an inherent attribute to model optimization and it was estimated to be at least 17% for the absorption of Chl a and 7% for the backscattering of TSM (Salama & Stein, 2009).

Conclusions

In this article, we estimated and analyzed the variations of SIOP in the equatorial coastal waters of the Berau estuary in East Kalimantan. The SIOP were derived from extensive in situ measurements of subsurface irradiance reflectance and water constituents combined with hydro-optical model inversion. The results were validated using in situ measurements and ocean color satellite observations. The following can be concluded from this work:

1. Moving from turbid near shore estuarine waters to clear off shore waters, we could distinguish three water types that differ in their composition, turbidity, and hence optical light absorption and scattering signatures.
2. The specific absorption coefficient of Chl a is relatively constant for the three types of waters with an average value of 0.024 m^2 mg^{-1}.
3. The specific backscattering coefficient of TSM varied from 0.003 m^2 g^{-1}, for clear deeper coastal waters, to 0.020 m^2 g^{-1}, for shallow turbid near shore waters.
4. The spectral slope exponent of CDOM absorption was found to be spatially homogenous and in the range of 0.011–0.015 nm^{-1} with an average of 0.012 $\pm$ 0.002 nm^{-1};

These observed values of SIOP form a corner stone for future estimation of TSM and Chl a concentration from remote sensing data in the Berau estuary and other tropical equatorial coastal waters.

References

Albert, A. & C. D. Mobley, 2003. An analytical model for substance irradiance and remote sensing reflectance in deep and shallow case-2 waters. Optics Express 11(22): 2873–2890.

Astoreca, R., K. Ruddick, V. Rousseau, B. V. Mol, J. Y. Parent & C. Lancelot, 2006. Variability of the inherent and apparent optical properties in a highly turbid coastal area: impact on the calibration of remote sensing algorithms. EARSeL eProceedings 5(1): 1–17.

Babin, M., D. Stramski, G. M. Ferrari, H. Claustre, A. Bricaud, G. Obolenski & N. Hoepffner, 2003. Variation in the light absorption coefficient of phytoplankton, nonalgal particles, and dissolved organic matter in coastal waters around Europe. Journal of Geophysical Research 108(C7): 3211.

Babin, M., D. Stramski, G. M. Ferrari, H. Claustre, A. Bricaud, G. Obolenski & N. Hoepffner, 2004. Variation in the light absorption coefficient of phytoplankton, nonalgal particles, and dissolved organic matter in coastal waters around Europe. Journal of Geophysical Research 108: 3211.

Bricaud, A., A. Morel & A. L. Prieur, 1981. Absorption by dissolved organic matter of the sea (yellow substances) in the UV and visible domains. Limnology and Oceanography 26: 43–53.

Carder, K. L., F. R. Chen, C. P. Lee, S. Hawes & D. Kamykowski, 1999. Semi-analytic MODIS algorithms for chlorophyll a and absorption with bio-optical domains based on nitrate-depletion temperatures. Journal of Geophysical Research 104(C3): 5403–5421.

Chang, C. G., T. D. Dickey, C. D. Mobley, E. Boss & W. S. Pegau, 2003. Toward closure of upwelling radiance in coastal waters. Applied Optics 42(9): 1574–1582.

D'Sa, E. J. & R. L. Miller, 2005. Bio-optical properties of coastal waters. In Miller, R. L., C. E. Del Castillo & B. A. McKee (eds), Remote Sensing of Coastal Aquatic Environments: Technologies, Techniques and Applications. Springer, Dordrecht.

D'Sa, E. J., C. Hu, F. E. Muller-Karger & K. L. Carder, 2002. Estimation of colored dissolved organic matter and salinity fields in case 2 waters using SeaWiFS: examples from Florida Bay and Florida Shelf. Journal of Earth System Science 111(3): 197–207.

de Haan, J. F., J. M. M. Kokke, A. G. Dekker & M. Rijkeboer, 1999. Remote sensing algorithm development: operationalisation of tools for the analysis and processing of remote sensing data of coastal and inland waters. NBN 90 54 11 267 0.

Dekker, A. G., 1993. Detection of optical water quality parameters for eutrophic waters by high resolution remote sensing. Ph.D. Thesis, Free University, Amsterdam, The Netherlands: 1–240.

Dekker, A. G., S. W. M. Peters, M. Rijkeboer & H. Berghuis, 1999. Analytical processing of multi-temporal SPOT and Landsat images for estuarine management in Kalimantan Indonesia. In Nieuwenhuis, G. J. A., R. Vaughan & M. Molenaar (eds), 18th EARSeL Symposium on Operational Remote Sensing for Sustainable Development. A.A. Balkema, Rotterdam: 315–324.

Doerffer, R. & J. Fischer, 1994. Concentration of chlorophyll, suspended matter, and gelbstoff in case II waters derived from satellite coastal zone color scanner with inverse methods. Journal of Geophysical Research 99(C4): 7457–7466.

Doerffer, R. & H. Schiller, 2007. The MERIS Case 2 water algorithm. International Journal of Remote Sensing 28: 517–535.

Gallegos, C. L. & D. L. Correl, 1990. Modelling spectral diffuse attenuation, absorption and scattering coefficients in a turbid estuary. Limnology and Oceanography 35: 1486–1502.

Gege, P., 2005. The water colour simulator WASI. User manual for version 3. DLR Internal Report IB 564-01/05: 83 pp.

Glantz, M., R. Katz & N. Nicholls (eds), 1991. Teleconnections Linking Worldwide Climate Anomalies. Cambridge University Press, Cambridge.

Gordon, H. R., 1991. Absorption and scattering estimates from irradiance measurements: Monte Carlo simulation. Limnology and Oceanography 36: 769–777.

Gordon, H. R. & A. Y. Morel, 1983. Remote Assessment of Ocean Color for Interpretation of Satellite Visible Imagery: A Review. Springer, New York.

Gordon, H. R. & M. Wang, 1994. Retrieval of water-leaving radiance and aerosol optical thickness over the oceans with SeaWiFS: A preliminary algorithm. Applied Optics 33: 443–452.

Gordon, H. R., O. B. Brown & M. M. Jacobs, 1975. Computed relationship between the inherent and apparent optical properties of a flat homogeneous ocean. Applied Optics 14: 417–427.

Gordon, A. L., R. D. Susanto & A. Ffield, 1999. Through flow within Makassar Strait. Geophysical Research Letters 26(21): 3325–3328.

Haltrin, V. I. & R. A. Arnone, 2003. An algorithm to estimate concentrations of suspended particles in seawater from satellite optical images. In I. Levin & G. Gilbert (eds), Current Problems in Optic Natural Waters. Proceedings of the II International Conference ONW, St. Petersburg, Russia.

Hamre, B., Ø. Frette, S. R. Erga, J. J. Stamnes & K. Stamnes, 2003. Parameterization and analysis of the optical absorption and scattering coefficients in a Western Norwegian fjord: a case II water study. Applied Optics 42: 883–892.

Hautala, S. L., J. Sprintall, J. T. Potemra, J. C. Chong, W. Pandoe, N. Bray & A. G. Ilahude, 2001. Velocity structure and transport of the Indonesian through flow in the major straits restricting flow into the Indian Ocean. Journal of Geophysical Research 106(C6): 19527–19546.

Hendiarti, N., H. Siegel & T. Ohde, 2004. Investigation of different coastal processes in Indonesian waters using SeaWiFS data. Deep Sea Research II 51: 85–97.

Hooker, S. B. & S. Maritorena, 2000. An evaluation of oceanographic radiometers and deployment methodologies. Journal of Atmospheric and Ocean Technology 17: 811–830.

Ibelings, B., R. Vos, P. Boderie, H. Hakvoort & E. Hoogenboom, 2001. The RALLY project: remote sensing of algal blooms in Lake IJssel – integration with in situ data and computational modeling. RIZA report 2001.036, RIZA Institute for Inland Water Management and Waste Water Treatment.

IOCCG, 2006. Remote sensing of inherent optical properties: fundamentals, tests of algorithms, and applications. In Lee, Z.-P. (ed.), Reports of the International Ocean-Colour Coordinating Group, No. 5. IOCCG, Dartmouth, Canada.

Jerlov, N. G., 1976. Marine Optics. Elsevier, Amsterdam. 231 p.

Kahru, M. & B. G. Mitchell, 2001. Seasonal and non-seasonal variability of satellite derived chlorophyll and colored dissolved organic matter concentration in the California current. Journal of Geophysical Research 106: 2517–2529.

Kirk, J. T. O., 1984. Dependence of relationship between inherent and apparent optical properties of water on solar altitude. Limnology and Oceanography 29: 350–356.

Kratzer, S., C. Brockmann & G. Moore, 2008. Using MERIS full resolution data to monitor coastal waters – a case study from Himmerfjärden, a fjord-like bay in the northwestern Baltic Sea. Remote Sensing of Environment 112: 2284–2300.

Le, C., Y. Li, Y. Zha & Y. Sun, 2009. Specific absorption coefficient and the phytoplankton package effect in Lake Taihu, China. Hydrobiologia 619: 27–37.

Maritorena, S., D. A. Siegel & A. R. Peterson, 2002. Optimization of a semi-analytical ocean color model for global-scale applications. Applied Optics 41: 2705–2714.

Matthew, M. W., S. M. Adler-Golden, A. Berk, S. C. Richtsmeier, R. Y. Levine, L. S. Bernstein, P. K. Acharya, G. P. Anderson, G. W. Felde, M. P. Hoke, A. Ratkowski, H.-H. Burke, R. D. Kaiser, D. P. Miller, 2000. Status of atmospheric correction using a MODTRAN4-based algorithm. SPIE Proceeding, Algorithms for Multispectral, Hyperspectral, and Ultraspectral Imagery VI, Vol. 4049.

Mercado, J. M., T. Ramírez, & D. Cortés, 2007. Changes in nutrient concentration induced by hydrological variability and its effect on light absorption by phytoplankton in the Alborán Sea (Western Mediterranean Sea). Journal of Marine Systems. doi:10.1016/j.jmarsys.2007.05.009.

Mitchell, B. G. & D. A. Kiefer, 1988. Variability in the pigment specific fluorescence and absorption spectra in the

northeastern Pacific Ocean. Deep Sea Research A 35: 665–689.

Morel, A., 1974. Optical properties of pure water and pure sea water. In Jerlov, N. G. & E. Steemann Nielsen (eds), Optical Aspects of Oceanography. Academic Press, London: 1–24.

Morel, A. & L. Prieur, 1977. Analysis of variations in ocean color. Limnology and Oceanography 22: 709–722.

Pope, R. M. & E. S. Fry, 1997. Absorption spectrum (380–700 nm) of pure water, II, integrating cavity measurements. Applied Optics 36: 8710–8723.

Preisendorfer, R. W., 1976. Hydrologic Optics. U.S. Department of Commerce, National Oceanic and Atmospheric Administration, Environmental Research Laboratories, Pacific Marine Environmental Laboratory.

Prieur, L. & S. Sathyendranath, 1981. An optical classification of coastal and oceanic waters based on the specific spectral absorption curves of phytoplankton pigments, dissolved organic matter, and other particulate materials. Limnology and Oceanography 26: 671–689.

Reynolds, R. A., D. Stramski & B. G. Mitchell, 2001. A chlorophyll dependent semi-analytical reflectance model derived from field measurements of absorption and backscattering coefficients within the Southern Ocean. Journal of Geophysical Research 106(C4): 7125–7138.

Salama, M. S. & F. Shen, 2010a. Stochastic inversion of ocean color data using the cross-entropy method. Optics Express 18(2): 479–499.

Salama, M. S. & F. Shen, 2010b. Simultaneous atmospheric correction and quantification of suspended particulate matter from orbital and geostationary earth observation sensors. Estuarine, Coastal and Shelf Sciences 86(3): 499–511.

Salama, M. S. & A. Stein, 2009. Error decomposition and estimation of inherent optical properties. Applied Optics 48: 4947–4962.

Salama, M. S., J. Monbaliu & P. Coppin, 2004. The atmospheric correction of AVHRR images. International Journal of Remote Sensing 25(7–8): 1349–1355.

Salama, M. S., A. Dekker, Z. Su, C. M. Mannaerts & W. Verhoef, 2009. Deriving inherent optical properties and associated inversion-uncertainties in the Dutch lakes. Hydrology and Earth System Sciences 13: 1113–1121.

Sathyendranath, S., L. Lazzara & L. Prieur, 1987. Variations in the spectral values of specific absorption of phytoplankton. Limnology and Oceanography 32(2): 403–415.

Sharkov, E. A., 1998. Remote Sensing of Tropical Region. John Wiley & Sons in association with Praxis Publishing, Chichester.

Smith, R. C. & K. S. Baker, 1981. Optical properties of the clearest natural waters (200–800 nm). Applied Optics 20: 177–184.

Stramski, D., A. Sciandra & H. Claustre, 2002. Effects of temperature, nitrogen, and light limitation on the optical properties of the marine diatom *Thalassiosira pseudonana*. Limnology and Oceanography 47: 392–403.

Susanto, R. D., T. S. Moore II & J. Marra, 2006. Ocean color variability in the Indonesian Seas during the SeaWiFS era. Geochemistry, Geophysics, Geosystem 7: Q05021. doi: 10.1029/2005GC001009.

Tilstone, G. H., G. F. Moore, K. Sørensen, R. Doerfeer, R. Røttgers, K. D. Ruddick, R. Pasterkamp & P. V. Jørgensen, 2002. Regional validation of MERIS chlorophyll products in North Sea coastal waters. REVAMP Methodologies EVGI-CT-2001-00049.

Van der Woerd, H. J. & R. Pasterkamp, 2001. A rigorous method to retrieve TSM concentrations from multi-temporal SPOT images in highly turbid coastal waters. 11ARSPC.